JOURNAL OF MATERIALS SCIENCE **34** (1999) 3755–3767

Melt processing and microstructural analysis of $GdBa_2Cu_3O_y$ with varying amounts of Gd_2BaCuO_5 phase

E. SUDHAKAR REDDY, T. RAJASEKHARAN
Defence Metallurgical Research Laboratory, Hyderabad 500 058, India
E-mail: treddy@hongo.ecc.u-tokyo.ac.jp

Bulk samples of $GdBa_2Cu_3O_y$ (Gd-123) with varying amount of Gd_2BaCuO_5 (Gd-211) phase are melt processed. The processing conditions and the resulting macro and microstructures were discussed. The T_c of the material is found to be sensitive to the processing atmosphere, and the percentage of 211 in the precursor powder. Pure Gd-123 samples behaved differently as compared to the compositions with excess 211 phase. The amount of porosity and the average size of pores in the samples decreases with the increasing amount of Gd-211 in the precursor powder. The densification of the melt textured material is ascribed to the densification process of the precursors prior to the texturing stage. Irrespective of the Gd-211 content macro-cracks within domains were observed in parallel to the intrinsic micro-cracks. At the melting stage refinement of the Gd-211 particles originating from the decomposition of Gd-123 was observed with the increasing amounts of external Gd-211 in the liquid. The quantitative analysis of the microstructural features, i.e., the residual Gd-211, platelet width, domain sizes of the resulting melt textured materials were presented. Addition of Ag resulted in mild refining of 211 particles.

1. Introduction

Since the discovery of $YBa_2Cu_3O_y$ (Y-123) high temperature superconductors, substantial amount of efforts have been made to enhance the critical current density (J_c) of the bulk material. The conventionally sintered Y-123 showed very low J_c's due to the misorientation and weakly coupled grains. The ab-plane alignment of grains were achieved by melt processing of the sintered 123 material [1]. Compared to the sintered material where grains are randomly oriented the J_c of the textured material is a few orders of magnitude higher [2, 3]. Further increase in J_c is obtained by arresting flux-creep by the introduction of pinning centres in bulk materials [4–7]. Of various inclusions which can contribute for flux pinning, Gd-211 particles emerged as good candidates for arresting the flux creep. The Gd-211 particles themselves with a typical size of few microns, are not found to aid for flux pinning whereas the secondary defects of the size of coherence length at interface of 123/211 are found to act as flux pinning centres [2, 8–10]. The amount of defects introduced into the material is dependent on the volume and the morphology of the 211 particles.

The role of 211 is not limited only to the flux pinning, it is also important to processing good and homogeneous textured material. Melt processing techniques generally involve melting of 123 above the peritectic temperature which is highly incongruent and results in solid 211 phase particles with barium cuprates and copper oxides as liquid phases. The liquid at this stage is highly viscous and out flows from the interior of the material. It is also highly corrosive and hence cannot be retained in any container. In order to have a uniform and continuous growth of 123, in the partially molten state, the material should be able to retain the liquids within the bulk. The liquid phase outflow can be eliminated by properly tailoring the homogeneity and density of the 211 particles in liquid phase at melting stage. And also, it is important to control the size and morphology of the 211 particles in the final microstructure for an effective flux pinning. Therefore a study of 211 content on various parameters during melt processing is very important for the optimisation of the bulk material with a good homogeneous macro- and microstructural features and hence better superconducting properties.

In this paper, we report on the study of melt processing of Gd-123 with varying amounts of Gd-211 phase. The processing parameters for the fabrication of samples with good superconducting properties are discussed. Quantitative analyses of the various macro- and microstructural features of the samples at different stages of processing are presented.

2. Experimental

Precursor powders of $GdBa_2Cu_3O_y$ and Gd_2BaCuO_5 in molar ratios $(100 - x)$: x, with $x = 0$, 10, 20, 30, 40,

and 30 mol% with 5 wt% Ag, (here after termed as Gd-0%, Gd-10%, Gd-20%, Gd-30%, Gd-40% and Gd-30% + Ag respectively) were prepared from high purity Gd_2O_3, $BaCO_3$ and CuO by a chemical route and subsequent vacuum calcination. The phase purity of the powders were confirmed by XRD. For processing of Ag containing composite, high purity commercially available Ag powder of particle size of 5–10 μm was mixed (5 wt%) with the Gd-30 mol% powder in an agate mortar for 4 hours. The precursor powders for melt processing were uniaxially pressed into pellets of size $15 \times 15 \times 7$ mm in a steel die under a pressure of 10 Ton. The pellets were melt processed in a tube furnace with a homogeneous hot zone of 5 cm around the thermocouple. The temperature accuracy within the hot zone is $\pm 0.5\,^{\circ}$C with respect to the set temperature. No vertical or lateral temperature gradients were measured within the space reserved for the sample. The specimens for microstructural investigations were selected from the surface of the samples and mounted in a cold setting epoxy resin and polished. The polished surfaces were observed using a Leitz Optical microscope equipped with a polariser, and JEOL JSM-840 scanning electron microscope. The representative regions were photographed. The micrographs were then analysed using standard quantitative metallographic methods [11]. The resistivity measurements were done by a four probe method employing conducting silver paint as electrical contacts.

3. Results and discussion

3.1. Melt processing

The initial attempts to melt process the samples in ambient atmospheres resulted in material with critical transition temperature (T_c), less than 90 K. Fig. 1 shows the normalised resistance vs. temperature curves for the samples Gd-0% and Gd-30%, processed in air. The T_c of the samples are 76 and 60 K with broad transition width for Gd-0% and Gd-30% respectively. The lower T_c of the material can be attributed to the formation of a solid solution compound of $Gd_{1+x}Ba_{2-x}Cu_3O_y$ similar to the one reported for Sm-123 and Nd-123 systems [12, 13]. The solid solution formation is promoted by the comparable sizes of Ba and Gd ions. The XRD patterns of the samples, after oxygenation, are shown in Fig. 2. An indication to the change from orthorhombicity to tetragonal structure of the 123 unit cell is the difference in the pattern of the (006), (020) and (200) reflections [14, 15]. The absence of the separate reflections for the peaks can be seen from the insets of Fig. 2a and b, which represents the existing of tetragonal structure due to the solid solution formation. The extent of solid solution varies with increasing size of RE-ion in RE-123 [16]. In the case of Gd-system solid solubility upto $x = 2.5$ was observed [16]. The solid solubility has been found to be suppressed by processing in partial oxygen atmospheres as reported for Sm-123 and Nd-123 in the OCMG process [12, 13, 16]. Following the work of Sm-123 and Nd-123 systems, we melt processed the Gd-123 samples in flowing high pure Ar (O_2 impurity: <2ppm) with a flow rate of 1 l/min. The melt processing of the composites was carried out using thermal schedule shown in Fig. 3. The pellets were first sintered at 910 °C for 6 h, and were rapidly heated to 1110 °C and held there for 20 minutes, cooled rapidly to 1015 °C and then slowly cooled to 910 °C at a rate of 1 °C/h. The resulting textured tetragonal 123 was transformed into the orthorhombic phase by annealing in flowing oxygen between 600–300 °C according to the schedule shown in the Fig. 3.

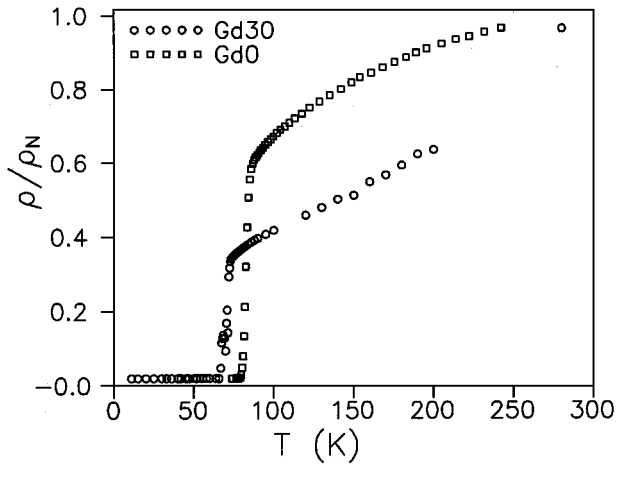

Figure 1 Temperature dependence of the electrical resistance of the samples Gd-0% and Gd-30%, processed in ambient atmosphere, after oxygenation.

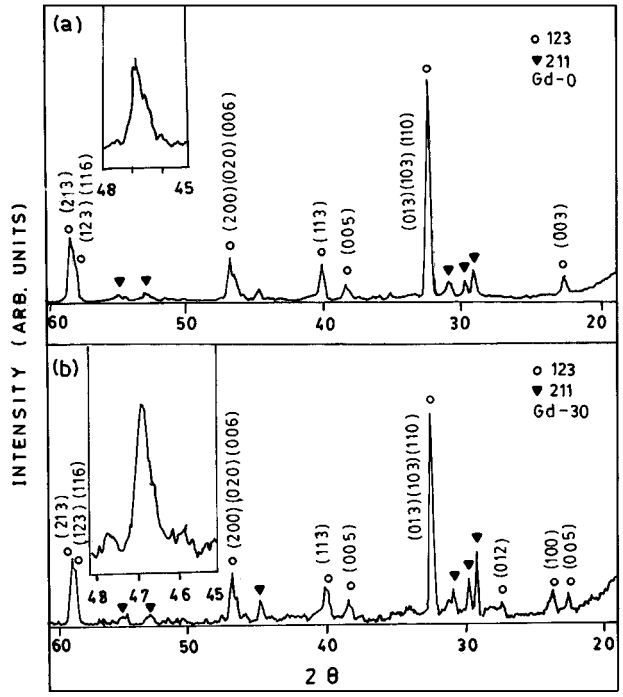

Figure 2 X-ray diffraction patterns from the samples discussed in Fig. 1. The absence of splitting of the peaks (020), (200) and (006) (inset shows the magnified portion) representing the tetragonal nature due to the solid solution formation can be seen.

3.2. Critical transition temperatures

The resistance of the samples were measured as a function of temperature as shown in Fig. 4. The T_c given in Table I. All the samples exhibited T_c greater than 90 K with a transition width less than 1.25 K, evidencing the

TABLE I The various microstructural features and transition temperatures obtained on melt textured $GdBa_2Cu_3O_y$ samples with varying amounts of Gd_2BaCuO_5 phase

Sample	Initial 211 (mol %)	$T_c(0)$	ΔT_c	Residual 211 (vol %)	Pro-peritectic 211 size (μm)	Residual 211 size (μm)	Platelet width (μm)
Gd-0	0	91.3	0.8	11.6	70	11.2	11
Gd-10	10	90.2	0.6	20.7	16	4.5	5.1
Gd-20	20	91.0	0.6	37.1	2.9	2.7	3.1
Gd-30	30	90.2	0.6	41.1	2.2	1.9	1.9
Gd-40	40	90.9	1.0	62.0	1.8	1.5	1.6
Gd-30 + Ag	30	91.4	0.8	42.1	—	1.0	1.1

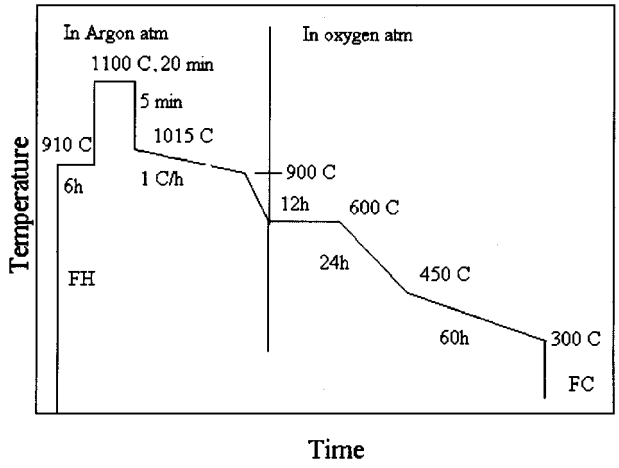

Figure 3 The time-temperature profile used for melt processing the samples in high pure Ar atmosphere. The right side of the dotted line represents the schedule used to oxygenate the samples.

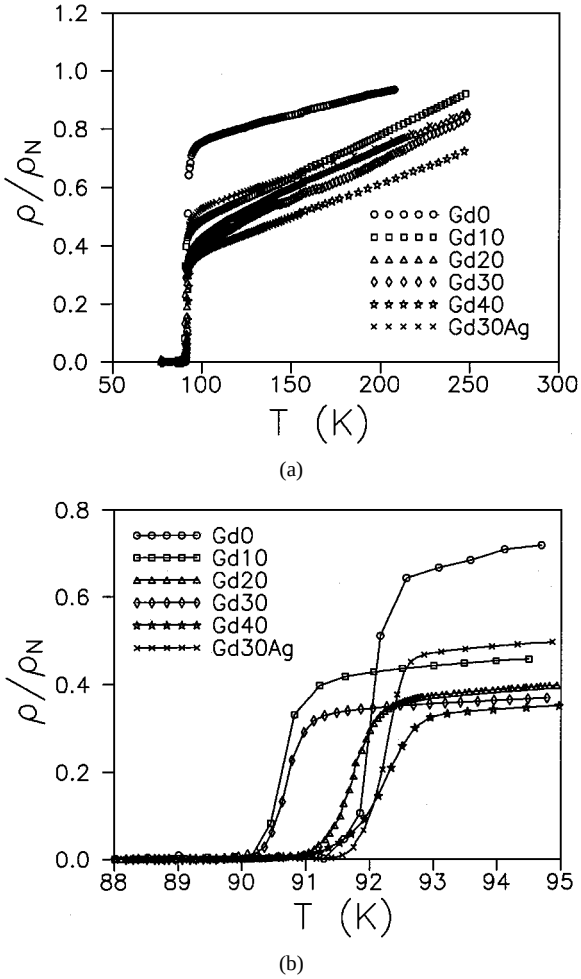

Figure 4 (a) Temperature dependence of the dc electrical resistance of the melt processed Gd-123 with varying amounts of Gd-211 phase. (b) Magnified portion of the curves near T_c.

suppression of solid solution formation by the processing method used in this work.

3.3. Gd_2BaCuO_5 particles at melting stage

To study the characteristics of 211 particles at the melting stage the pellets, after melting at 1100 °C for 20 min were quenched to room temperature onto a copper block. The decomposition of 123 at 1100 °C leads to formation of Gd-211 and liquid consisting of barium cuprates and copper oxide, that is

$$123 \rightarrow 211 + \text{liquid}$$

Fig. 5a–e shows the microstructures of samples with varying amounts of Gd-211 quenched from 1110 °C. It was observed that the morphology of the Gd-211 particles changed from acicular to spherical shape with increasing Gd-211 concentration. The presence of even a small percentage (10 mol %) of extra Gd-211 changed the morphology of the Gd-211 particles as compared to sample with stoichiometric composition. Further increase in Gd-211 content has less effect on morphology and size of the Gd-211 particles. Fig. 6 shows a plot of average size of the Gd-211 particles at the melting stage with respect to Gd-211 content in the starting compositions. The sizes of Gd-211 particles are measured directly from the micrographs, which is the average of the longest dimensions of the particles.

The change in morphology of the Gd-211 particles and the reduction in grain size can be explained in the following way: It is difficult to confirm metallographically, if the pre-existing Gd-211 particles and the peritectically formed Gd-211 particles are of the same rare earth element, whether the pre-existing Gd-211 particles in the liquid acts as nucleating substrates for the peritectically formed Gd-211 particles. In a study of the effect of externally added Er-211 on the microstructure of melt processed Y-123 [17, 18], it was observed that Y-211 formed on pre-existing Er-211 particles, with Er-211 as its core during the peritectic reation. This was revealed by back-scattered images. Hence, in the present case also the pre-existing Gd-211 particles in the liquid at the melting stage can be assumed to act as nucleating substrates for the Gd-211 particles formed during the decomposition of 123.

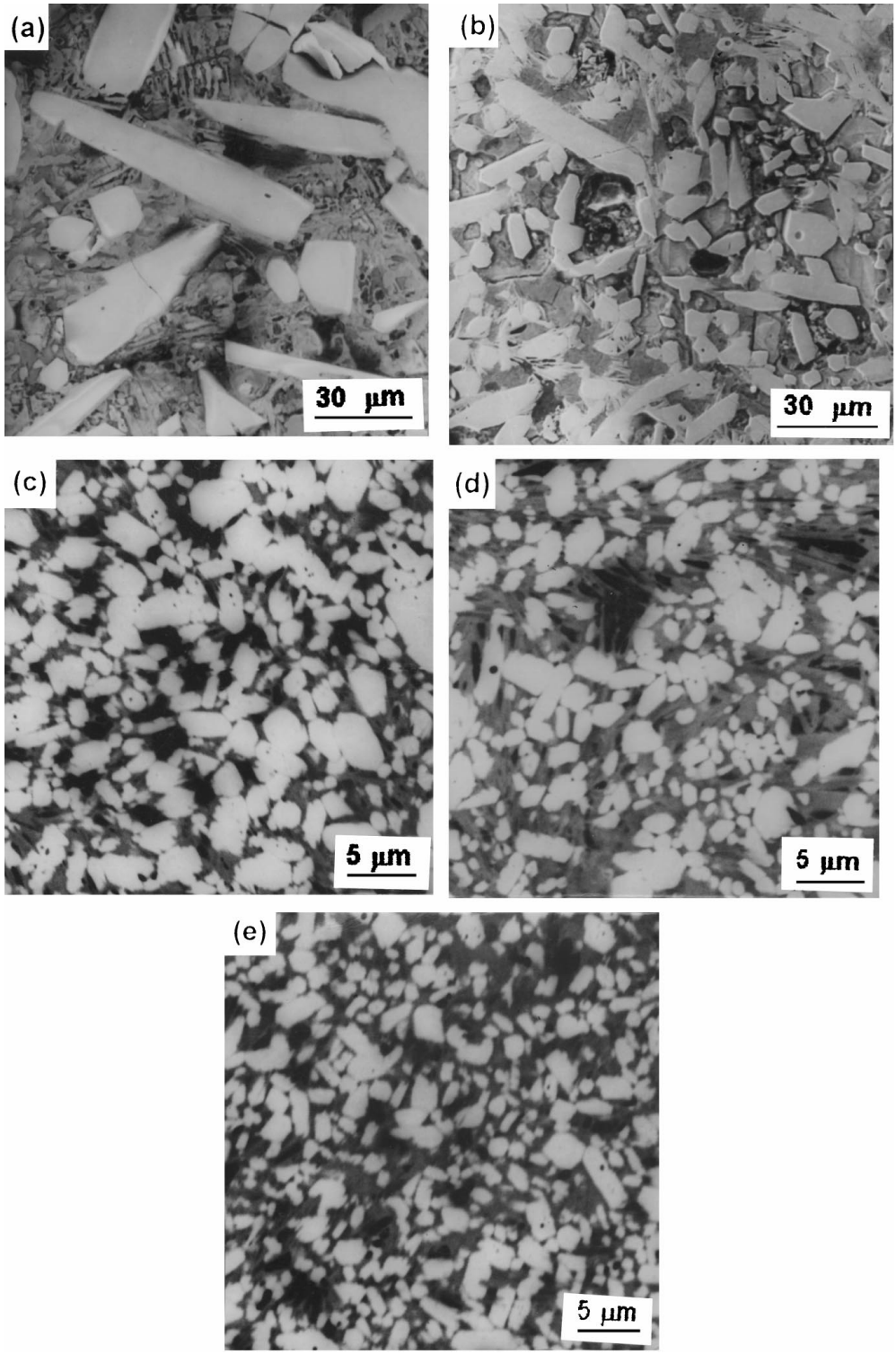

Figure 5 SEM photomicrographs showing Gd-211 particles in liquid matrix in Gd-123 samples quenched from 1100 °C after a hold of 20 minutes, containing, (a) 0, (b) 10, (c) 20, (d) 30 and (e) 40 mol % Gd-211.

In the samples with stoichiometric composition of Gd-123, the Gd-211 particles, formed by decomposition of 123, grows on a very small number of nuclei. Since there is enough space in liquid for such nuclei to grow freely without impinging on one another, they grow in their natural prismatic habit. In samples with extra Gd-211, the pre-existing Gd-211 particles serve as substrates for the nucleation of Gd-211 formed by 123 decomposition, and the Gd-211 phase distribute to a large number of nuclei, leading to decrease in the average size of Gd-211 particles. Hence with the increasing amount of externally added Gd-211 particles i.e., with more number of nucleating sites, the average size of the Gd-211 particles formed from the decomposition of 123 decreased.

3.4. Macrostructure

One of the major difficulties associated with the use of melt grown materials in applications is the difficulty to form useful shapes simultaneous with high J_c. The fact that melt processing is done in the presence of a

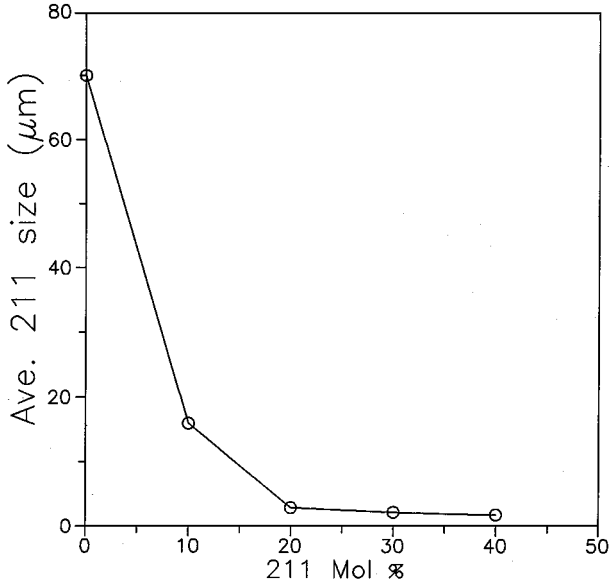

Figure 6 The average Gd-211 size at the melting stage versus the Gd-211 concentration in the starting precursor material.

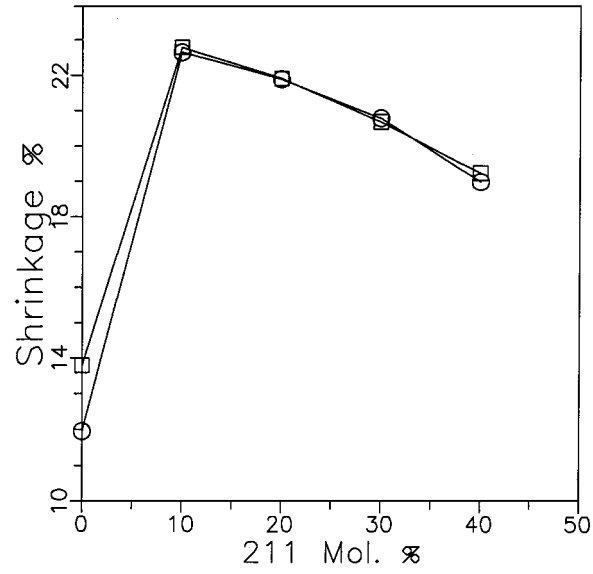

Figure 7 Plot showing the percentage of lateral shrinkage of Gd-123 samples, after melt processing (circles) and at melting stage (squares). The curves are similar and the values are also very close. The shrinkage occurs during the melting stage, and very little during subsequent peritectic reaction.

large quantity of liquids cause a substantial amount of shrinkage (∼20%) in the final product. This shrinkage and the flowing out of liquids cause cracking, distortions and voids in the interior of the material. In the present section, various macro-structural defects like the shrinkages with associated distortions, porosity, and macro-cracks are systematically studied in melt processed Gd-123 as reinforced with various amounts of Gd-211 particles. The aim was to isolate the causes with a view to minimise them.

3.4.1. Shrinkage

To process any component into near-net shapes it is very important to have a knowledge of the shrinkages involved during processing. In the first instance, we studied the dimensional changes of the melt textured composites in variation with the Gd-211 content. In Fig. 7 the curve with circles represent the percentage of shrinkage in the lateral dimensions of melt processed samples as a function of Gd-211 content. It can be seen from the graph that shrinkages of the samples with 10–40 mol % Gd-211 varied nearly linearly, whereas the stoichiometric sample did not fit on the linear curve and behaved differently. To see whether the dimensional changes have occurred during texturing or at the stage of melting at 1100 °C, the samples were quenched after melting to room temperature and the dimensional changes were measured. The curve with squares in Fig. 7 shows the percentage of shrinkage in the lateral dimensions of the quenched samples. It can be seen from Fig. 7 that a very little shrinkage occurs subsequently during texturing. It can also be seen that the stoichiometric sample shrinks by only about 12–14%, whereas the presence of 10 mol % of Gd-211 increases the shrinkage dramatically to around 20%. Further increase of Gd-211 makes only relatively small changes in the shrinkage.

A possible mechanism, that explains the observed shrinkage with increasing Gd-211 content is suggested below: The pressed material when melted shrinks under the surface tensional forces exerted by the newly generated liquid, eliminating voids within. Shrinkage is related to the packing behaviour of the skeleton of Gd-211. In case of the stoichiometric sample, the Gd-211 particles are acicular with a large aspect ratio as found in the earlier section (Fig. 5). They do not pack well. Shrinkage is only 12–14%. In the Gd-211-rich samples (10–40 mol %), the Gd-211 are near spherical and are small in size (Fig. 5). With small size and spherical morphology the Gd-211 particles packs well and the shrinkage is nearly 20%.

3.4.2. Pores

Fig. 8a–e show the optical micrographs of the polished surfaces of melt processed samples, with increasing Gd-211 content, taken under polarised light. As there was no imposed temperature gradient on the samples, domains of 123 with different orientations (shadings) can be seen. The domains are of sizes ranging from 3×3 mm^2 to 10×10 mm^2. It can be seen that the samples have more or less uniformly distributed pores within them. The average size of the pores was estimated from the micrographs and plotted as a function of the Gd-211 concentration in Fig. 9. The pore size was ∼70–80 μm in the stoichiometric 123; the addition of just 10 mol % Gd-211 brought down the pore size substantially. Reduction in pore size with further increase in Gd-211 was to a lesser extent. The behaviour in Fig. 9, of pore size with increasing Gd-211 content, is similar to shrinkage. Both have a sharp variation in going from stoichiometric sample to the one with 10 mol % Gd-211, but a much slower variation subsequently.

The origin of the pores in melt processed Y-123 has been attributed to the following reasons in literature [19.20]: Kim *et al*. reported the origin of these pores

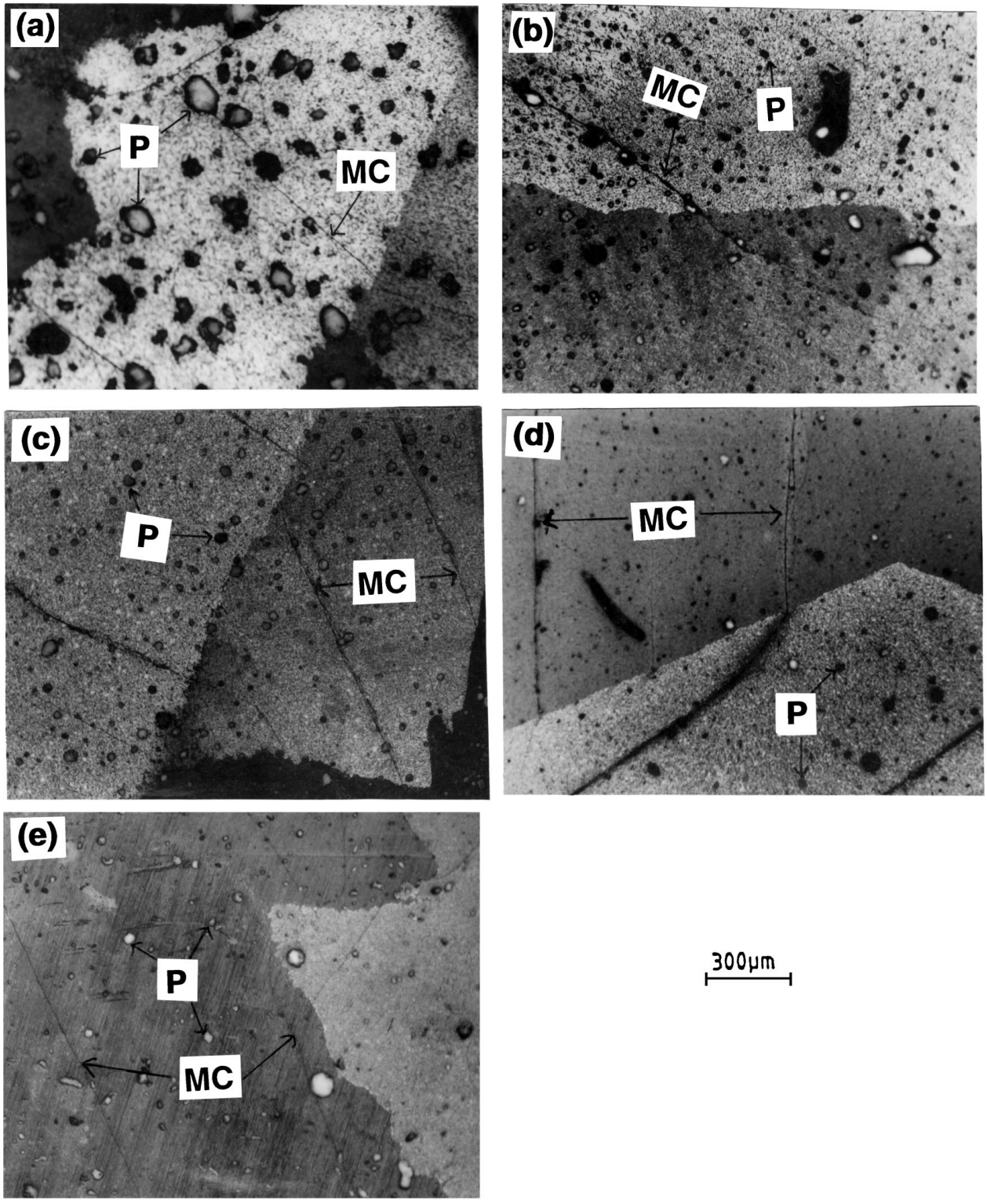

Figure 8 Representative micrographs of the polished surfaces of melt processed Gd-123 with varying amounts of Gd-211 content (a) 0, (b) 10, (c) 20, (d) 30 and (e) 40 mol % Gd-211, taken under polarised light. The different shadings of the domains represents their misorientation with respect one another. (P = Pores, MC = cracks)

as due to the evolution of gases from the bulk material during the melting stage at above T_p according to the equation

$$2GdBa_2Cu_3O_7 \rightarrow Gd_2BaCuO_5 + BaCuO_2 + 2CuO$$

and

$$2CuO \rightarrow Cu_2O + 1/2O_2 \uparrow .$$

But there exists no explanation for the gradual decrease in the pore size with increase in Gd-211 content. The increase in the Gd-211 volume can bring the following changes in the melting. The inter particle spacing will be decreased and the presence of more Gd-211 in the liquid can contribute for holding of the liquid phases in a better way, preventing the draining out of the liquid phases from the bulk. Although there is a possibility for the origin of pores due to the evolution of gases (from

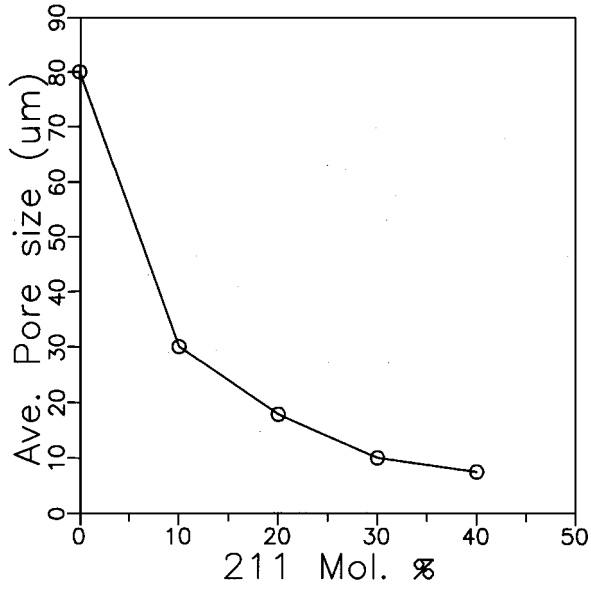

Figure 9 Plot showing the variation of the average pore size with the increasing amounts of Gd-211.

the melt), the exact size of the pores left by the gas packets is not clear. The decrease in pore size with increasing Gd-211 content can be attributed to the difference in the packing fraction of Gd-211 in the sample. The flowing out of liquids from the bulk may also contribute to the formation of pores to some extent.

The pores which we are seeing after melt processing may not be really pores and filled by liquid phases which were etched out during polishing. At the melting stage these pores may be filled by liquid phases and during the texturing stage, some times these liquid phase pools are converted into 123 phase by diffusion of solute ions from the neighbouring regions (Fig. 10), where as some times some amount of liquids will be frozen in these pores due to the nonavailability of RE-ions. The low solubility of RE-ions in liquid will also retard the transport of RE-ions to long distances and hence some times the liquid pools are not completely converted into 123 phase.

3.4.3. Cracks

Another serious defect that has to be eliminated before the melt textured materials can be put to practical use are macro-cracks. In Fig. 8, it can be observed that parallel cracks (marked as 'MC') are present in all the domains and also in all samples independent of the Gd-211 content. A closer examination of the micrographs published in the literature indicates that macro-cracking occurs universally in materials prepared by various melt processing techniques [21–26]. The cracks can be observed to be parallel within a domain. They are observed to extend from one end to the other in the domains. It is observed that the density of macro-cracks is more or less independent of the Gd-211 content in the present study. Some examples of the cracks occurring in samples with extra Gd-211 are shown in Fig. 11, at a high magnification. The cracks are observed to be parallel with the intrinsic micro-cracks (gaps) present in between the platelets. The main differences between the present macro-cracks and the inter-platelet gaps are that the macro-cracks are observed to be continuous and to crack the Gd-211 particles i.e., the reinforcement as they pass through. As the inter-platelet gaps are known to be in *ab* plane, the macro-cracks can be concluded to be in the same *ab* planes. No cracks were observed parallel to *c*-axis. This may be due to the anisotropy in the fracture toughness values i.e., $K_c(001) \ll K_c(100) \gg K_c(010)$ [27].

According to one of the hypotheses in the literature [28] the macro-cracks are described to occur due to the difference in the thermal expansion between the large islands of secondary liquid phases and 123. In the present case, particularly in Gd-211-rich cases, the samples are free from liquid phases and the above reason may not be appropriate. Another reason that has been proposed is the mismatch in thermal expansion coefficient between Gd-211 particles and 123 [29]. The independence of the density of cracks on the Gd-211 content points that the above reason as not applicable. One possible reason is thermal shocks for the formation of macro-cracks; but even very slowly cooled samples revealed almost the density of such cracks as fast cooled

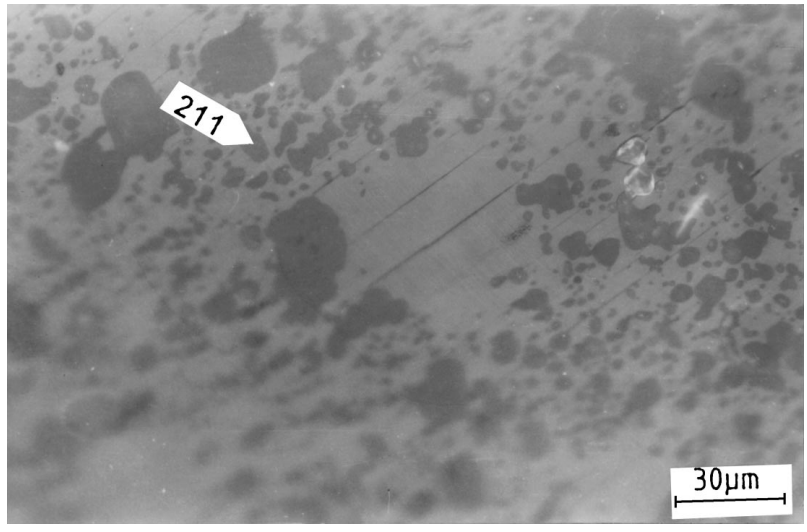

Figure 10 Optical micrograph showing a typical pore (Gd-211 free region) converted into 123 phase.

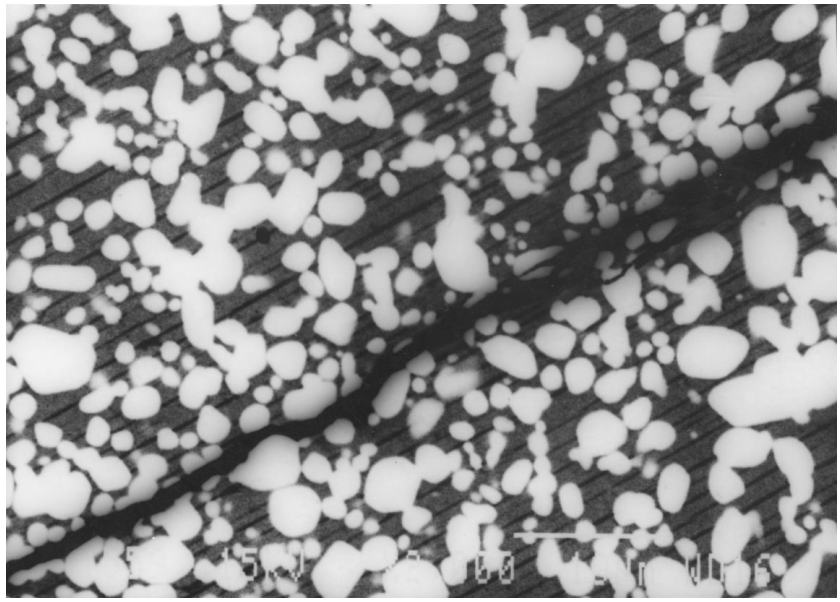

Figure 11 SEM micrographs of a Gd-211 rich sample showing crack propagation, at high magnification. The crack can be seen to break the Gd-211 particles through which it proceeds. The crack can be seen to be in parallel with the platelet gaps.

samples rendering this reason improbable. We observed that even tetragonal samples displayed the same density of macro-cracks as do the oxygen richer orthorhombic specimens, this suggesting that the tetragonal to orthorhombic transformation plays only a minimal role in providing the stresses for macro-cracking. Another possible reason for the cracks is the anisotropy in the thermal expansion coefficients of 123 domains which are held firmly and are differently oriented in the final material. In any case, unlike the inter-platelet gaps, which are more regular, the macro-cracks occur due to stresses after solidification.

3.5. Microstructure

3.5.1. Domains

In Fig. 8, the different levels of illumination under the polarised light reflects the fact that the domains are oriented in different directions. The size of the domains range from around $3 \times 3\ mm^2$ to $10 \times 10\ mm^2$. No systematic variations in the domain sizes were observed with increasing Gd-211 content.

3.5.2. Microstructural features within a domain

The important microstructural changes observed with increasing amount of Gd-211 concerns the features within the domains. Figs 12 and 13 show regions within the domains at higher magnifications for samples with varying amount of Gd-211. At the first instance, an increase in the volume percent and a decrease in size of residual Gd-211 particles can be noticed. The exact volume percent of the residual Gd-211, calculated using standard metallographic methods [11] and averaged over several micrographs, are given in Table I. An increase in the Gd-211 volume in comparison with the volume of extra Gd-211 added (Table I) in the precursor material can be observed. This may be due to the incomplete peritectic reaction or due to some amount of liquid phase loss in molten state.

Fig. 13 shows the variation in average size of the residual Gd-211 particles after melt processing, as a function of the increasing Gd-211 content. It can be seen that the size and morphology varies with the increase in the Gd-211 content. Similar phenomenon was also observed by other researchers in the Y-123 system but there exists no explanation for the above phenomena in the literature [2, 30]. The gradual decrease in Gd-211 particle size with increasing amounts of Gd-211 phase observed in the samples after texturing can be attributed to decrease in Gd-211 size at melting stage itself, which has been observed in Figs 5 and 6.

The other microstructural features observed to vary with the increase in Gd-211 content are the average thickness of the platelets, and the gap width between the platelets. Fig. 14 shows the variation in the platelet width with Gd-211 content. Fig. 15 shows the variation of the interplatelet gaps as a function of the Gd-211 concentration. The behaviours are similar to the one observed for the variation of the average size of the residual Gd-211 particles as function of Gd-211 concentration in Fig. 13. When the platelet thickness is plotted (Fig. 16) against the average size of the residual Gd-211 particles, a linear variation is observed. This is similar to the observation reported in the literature [2] on the Y-123 system where also a linear dependence of the platelet thickness on the average Gd-211 size was observed. Fig. 17 shows a plot of the interplatelet gap width with the platelet width. Within the measurement accuracy a linear dependence between the two can be observed, just as in the Y-123 system [2, 30].

It is interesting to note that the variations of the shrinkage on melt processing and porosity with Gd-211 concentration which were earlier connected to the nature and distribution of the primary phase particles in the liquid at 1100 °C in Section 3.4, is similar to that of

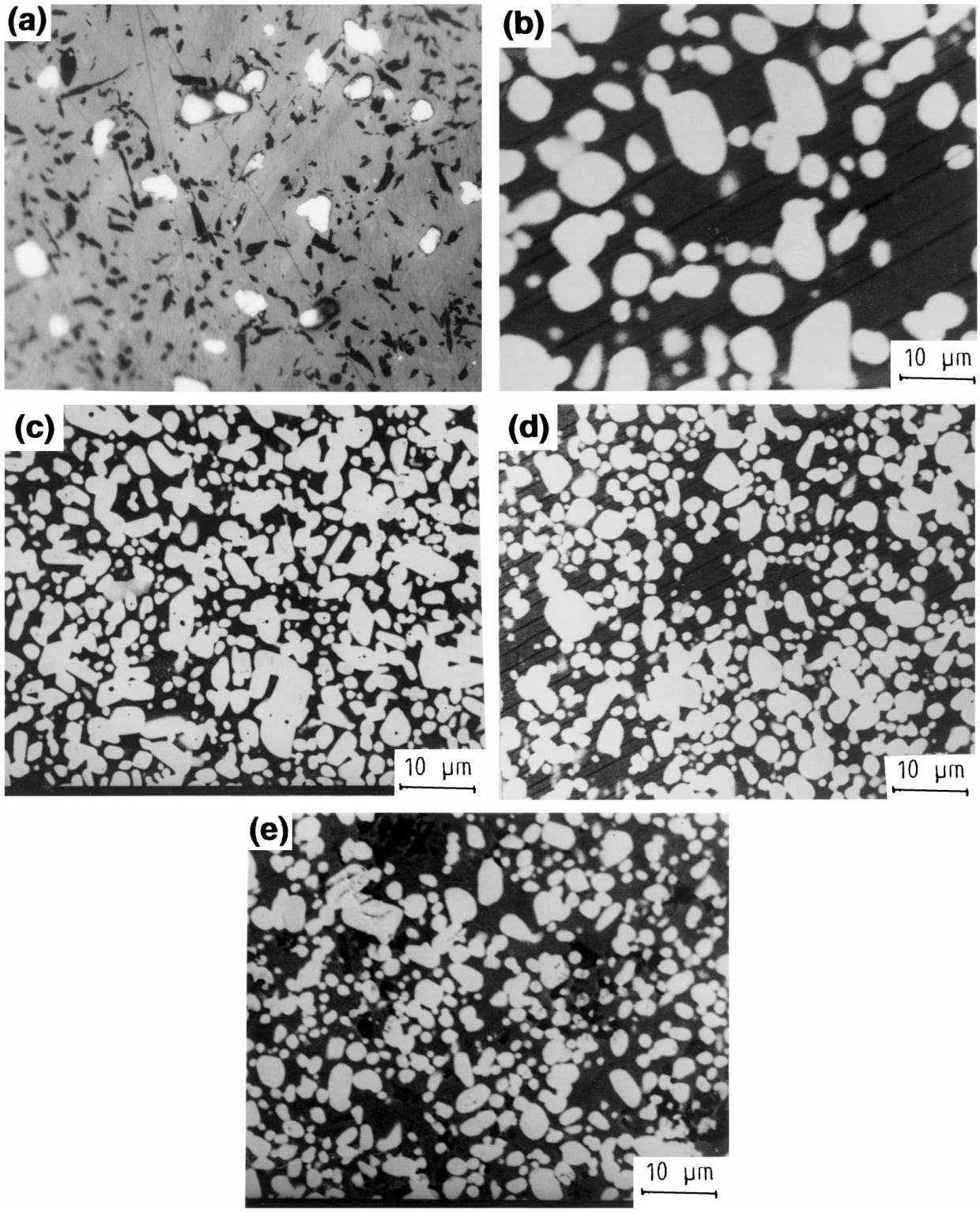

Figure 12 SEM micrographs of the polished region within domains for the samples: (a) Gd-0% (b) Gd-10% (c) Gd-20% (d) Gd-30% and (e) Gd-40%.

the platelet width, of the inter-platelet gap width and of the size of the residual Gd-211 particles with Gd-211 concentration.

3.6. Effect of Ag on $GdBa_2Cu_3O_y/Gd_2BaCuO_5$ composite

One of the few metals which have been found to be chemically inert and compatible with 123 without degrading its superconducting properties is Ag. Ag is found to improve the mechanical properties of the 123 matrix [31] and to refine its microstructure [2]. In the following section the results of the effect of Ag addition on the microstructure of melt processed $GdBa_2Cu_3O_y/Gd_2BaCuO_5$ (Gd-30%) composite as compared to a sample without Ag are discussed.

Fig. 18 shows an optical micrograph obtained using polarized light, of the melt processed Gd-30% + Ag sample. Two domains with different shades reflecting their mutually different orientations can be seen. The bright particles in the microstructure are silver and the small grey particles distributed all over the

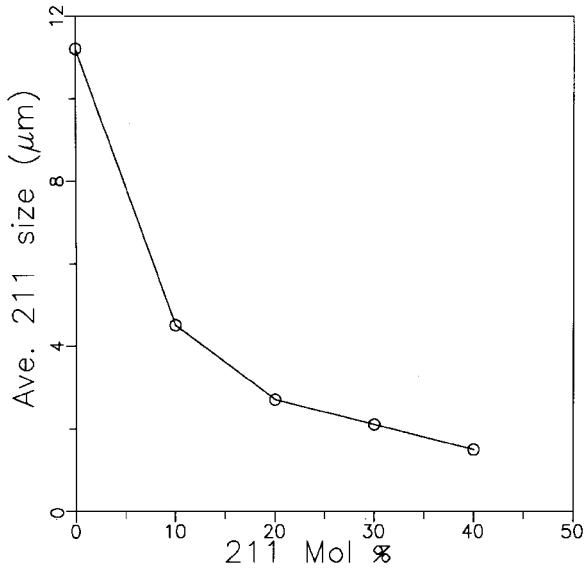

Figure 13 A plot showing the variation in the average size of the residual Gd-211 particles after melt processing with respect to the mol % of Gd-211.

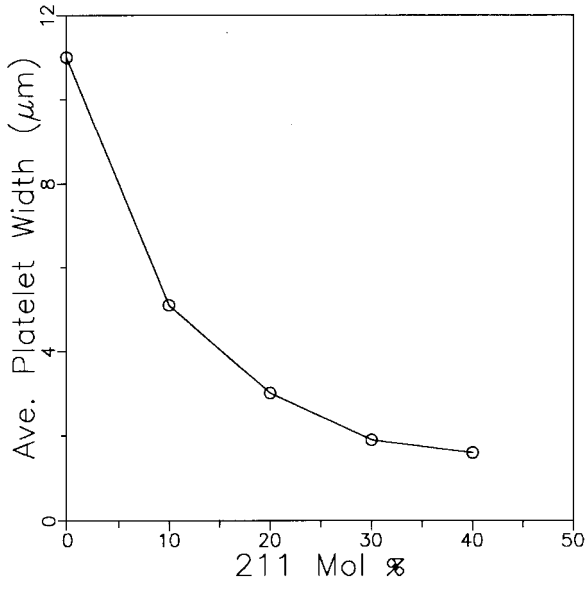

Figure 14 Plot showing the variation in the platelet width with respect to the starting Gd-211 content.

microstructure are Gd-211. Most of the silver particles are observed to have sizes in the range 5–10 μm.

An important observation from Fig. 18 is that of a refinement in the size of the Gd-211 particles by Ag addition. Fig. 19a and b show the SEM micrographs of the Gd-123/Gd-211 samples with and without Ag addition taken at a high magnification (see also Fig. 20). Quantitatively estimated distributions of the Gd-211 particles are shown in Fig. 21. It has been reported in the literature that the addition of other noble metals like Pt also refines Gd-211 particle size [32, 33]. As compared to Pt addition Ag is not found to be as effective in refining the Gd-211 particles as Pt.

A close observation of the Ag containing sample reveals a few more microstructural features. One of them is the occurrence of Gd-211-free regions around coarse Ag particles as shown in Fig. 22. The smaller Ag particles are found to be rather uniformly distributed among

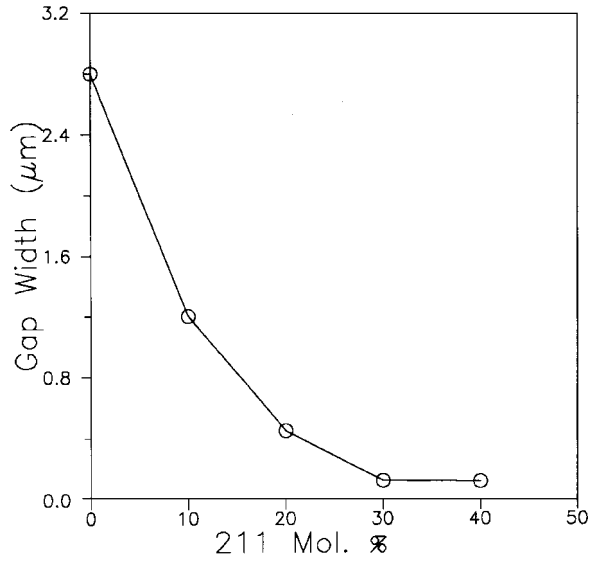

Figure 15 A plot of the average inter-platelet gap versus the starting Gd-211 content.

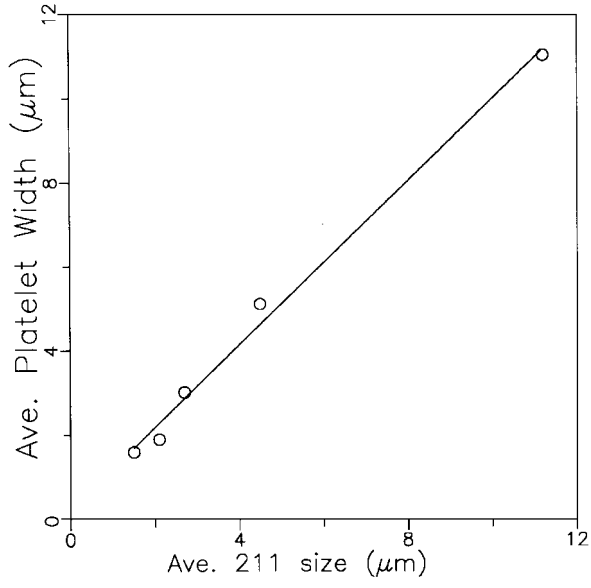

Figure 16 A plot showing the average platelet thickness with respect to the average size of the residual Gd-211 particles.

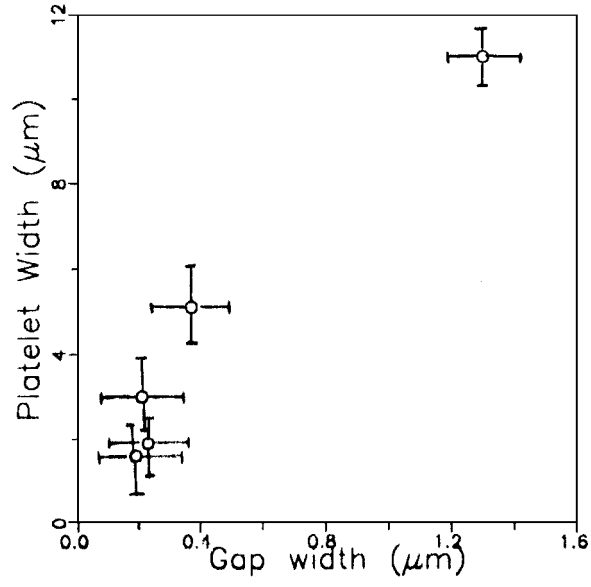

Figure 17 A plot between the Platelet width and Gap width between the platelets.

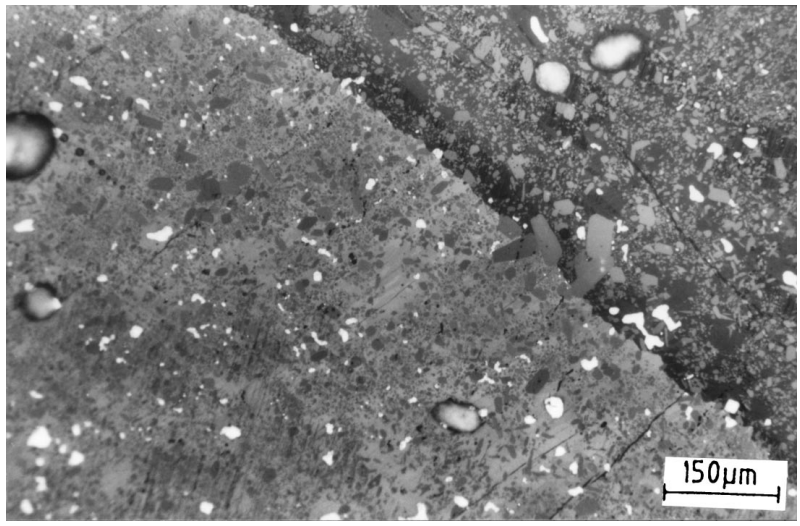

Figure 18 Optical micrograph of the melt processed Gd-123/211-Ag composite, taken under polarized light showing two differently oriented domains of 123. The shining particles are Ag and the small spherical, grey particles are Gd-211.

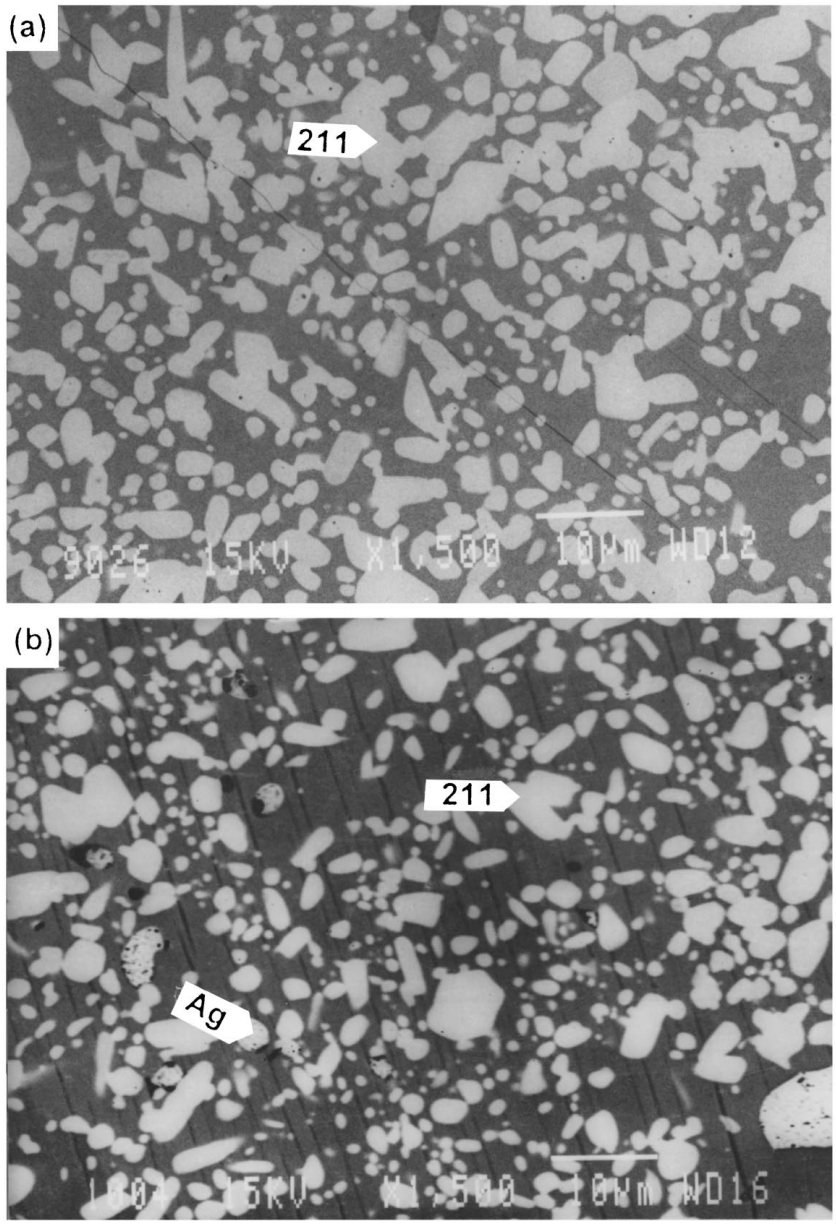

Figure 19 SEM photomicrographs of the composites: (a) without silver and (b) with Ag, showing the distribution and morphology of the residual Gd-211 particles in the matrix. The decrease in Gd-211 size as a result of Ag addition can be seen.

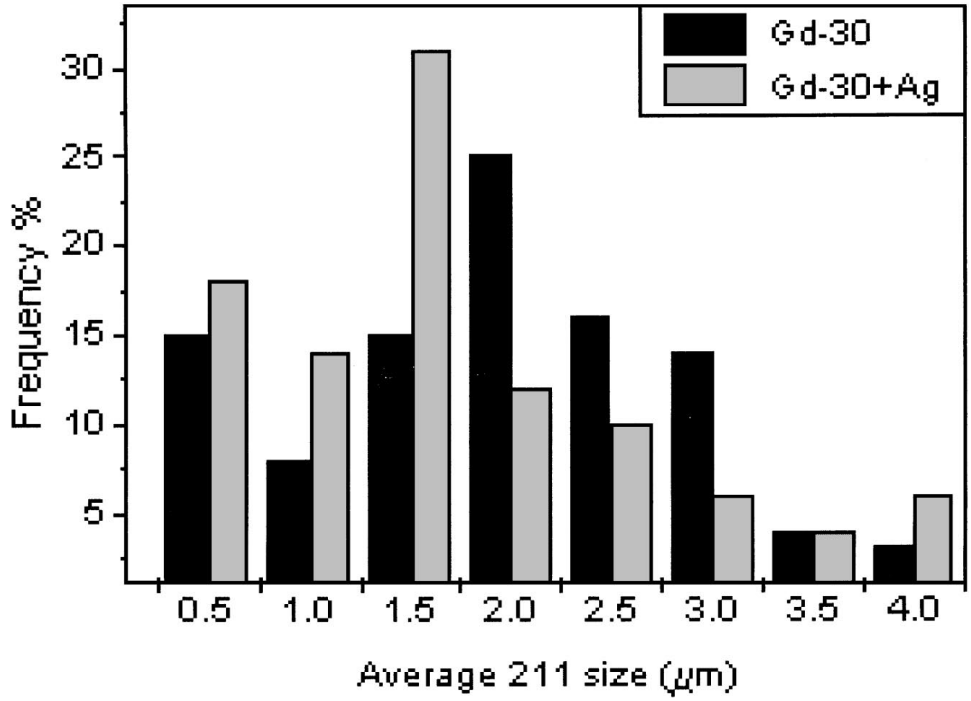

Figure 20 Histograms of the size of the residual Gd-211 particles present in the 123 matrix of the composites with and without Ag.

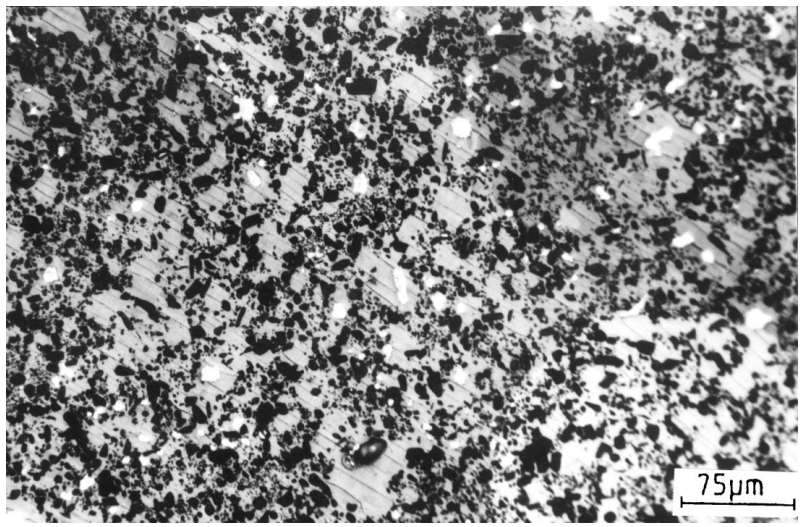

Figure 21 Optical micrograph of the Ag containing composite. Gd-211 free regions (marked) around coarse Ag particles can be seen.

the Gd-211 particles, whereas the coarser Ag particles, of the size 25–30 μm, are found in the Gd-211-free regions.

A possible mechanism for the formation of large Ag particles as a core for Gd-211-free regions can be explained on the basis of the pore formation as discussed in Section 3.4.2. The pores are formed at the melting stage. These pores are later filled with liquid phases in the molten state. At this stage, as the temperature is nearly 150 °C higher than the melting point of Ag, the liquid phases along with some amount of molten Ag will fill these pores. During the texturing stage, when cooling through T_p, these liquid phase pools will be converted into 123 by diffusion of RE-ions from the neighbouring regions, with Ag solidifying at the centre of the pores resulting in Gd-211 free regions with silver at the centre. For an effective and homogeneous pinning of the flux and for better mechanical properties, the above microstructural defect may not be desirable. The above microstructural defect has been eliminated by a modification of processing technique and is reported elsewhere [34].

Various quantities estimated from the microstructure are presented in Table I. The platelet thickness is observed to decrease with the addition of Ag as also the width of the gap between the platelets as compared to the samples without silver addition.

3.7. Summaries

$GdBa_2Cu_3O_y$ with various amounts of Gd_2BaCuO_5 phase (0 to 40 mol %) were melt processed. The processing atmosphere and temperature schedules were presented. All the resulting composites exhibited

$T_c > 90$ K with sharp transition widths (<1.25 K), in the electrical resistivity versus temperature measurements, showing the absence of solid solution formation.

The role of Gd-211 on the macro- and microstructural development, has been systematically studied. The densification of the samples is promoted by reinforcing with Gd-211 particles. The Gd-211 particles are effective in decreasing the porosity in the bulk material. The presence of macro-cracks within domains are observed to be independent of Gd-211 content and processing parameters.

The morphology of Gd-211 particles formed during the peritectic decomposition of stoichiometric 123 at 1100 °C is found to be acicular with large aspect ratio. The presence of external Gd-211 particles in the melt at the melting stage are very effective in modifying the morphology and refining the Gd-211 particles formed during the decomposition of 123, by acting as nucleation substrates.

The pore size is found to be inversely proportional to the pre-existing Gd-211. Other microstructural features i.e., the residual Gd-211 particle size, platelet thickness, gap width, were observed to be proportional to the amount of Gd-211 phase added and the average size of Gd-211 particles formed at the melting stage. The phenomena of decrease in Gd-211 particle size in the textured material with increasing amounts of Gd-211 phase in the starting composition is attributed to the decrease in Gd-211 size at the melting stage itself. The addition of Ag to Gd-30% resulted in the refinement of Gd-211 particles after melt processing.

Acknowledgements

The authors are grateful to the Director, DMRL, for permission to publish this work. ESR thanks the UGC for a fellowship.

References

1. S. JIN, T. H. TIEFEL, R. C. SHERWOOD, R. B. VAN DOVER, M. E. DAVIS, G. W. KAMMLOTT and R. A. FASTNACHT, *Phys. Rev.* **28** (1989) 1189.
2. R. GOPALAN, T. ROY, T. RAJASEKHARAN, G. RANGARAJAN and N. HARI BABU, *Physica C* **244** (1995) 106.
3. P. J. KUNG, M. P. MALEY, M. E. MCHENRY, J. O. WILLIS, M. MURAKAMI and S. TANAKA, *Phys. Rev. B* **18** (1993) 13922.
4. M. MURAKAMI, S. GOTOH, N. KOSHIZUKA, S. TANAKA, T. MATSUISHITA, S. KAMBE and K. KITAZAWA, *Cryogenics* **30** (1990) 390.
5. K. E. SICKAFUS, J. O. WILLIS, P. J. KUNG, W. B. WILSON, D. M. PARKIN, M. P. MALEY, F. W. CLINARD, C. J. SALGADO, R. P. DYE and K. M. HUBBARD, *Phys. Rev. B* **46** (1992) 11862.
6. R. B. VAN DOVER, E. M. GYORGY, L. F. SCHNEEMEYER, J. W. MITCHELL, K. V. RAO, R. PUZNIAK and J. V. WASZCZAK, *Nature* **343** (1989) 55.
7. P. MULLER, W. SCHINDLER, G. SAEMANN-ISCHENKO, H. BURZLAFF, H. GERSTENBERG and M. FISHER, *Physica C* **153–155** (1988) 343.
8. Z. L. WANG, A. GOYAL and M. KROEGER, *Phys. Rev. B* **47** (1993) 5373.
9. M. MIRONOVA, D. F. LEE and K. SALAMA, *Physica C* **211** (1993) 188.
10. D. F. LEE, M. MIRONOVA, V. SELVAMANICKAM and K. SALAMA, *Interface Sci.* **1** (1994) 381.
11. "The Basis of Quantitative Metallography," edited by F. B. Pickering, Institute of Metallurgical Technicians, Monograph No. 1.
12. S. I. YOO, N. SAKAI, H. TAKAICHI, T. HIGUCHI and M. MURAKAMI, *Appl. Phys. Lett.* **65** (1994) 633.
13. E. A. GOODILIN, N. N. OLEYNIKOV, E. V. ANTIPOV, R. V. SHPANCHENKO, G. Y. POPOV, V. G. BALAKIREV and Y. D. TRETYAKOV, *Physica* **272** (1996) 65.
14. M. SANO, Y. HAYAKAWA and M. KUMAGAWA, *Supercond. Sci. Technol.* **9** (1996) 478.
15. P. YOSSEFOV, G. E. SHTER, G. M. REISNER, A. FRIEDMAN, Y. YESHURUN and G. S. GRADER, *Physica C* **275** (1997) 299.
16. M. MURAKAMI, N. SAKAI, T. HIGUCHI and S. I. YOO, *Supercond. Sci. Technol.* **9** (1996) 1015.
17. C. VARANASI and P. J. MCGINN, *J. Electron. Mater.* **23** (1994) 1143.
18. D. BALKIN, C. VARANASI and P. MCGINN, in Proceedings of Spring MRS meeting, 1992.
19. C. J. KIM, H. G. LEE, K. B. KIM and G. W. HONG, *J. Mater. Res.* **9** (1995) 2235.
20. H. W. PARK, K. B. KIM, K. W. LEE, H. KUK, G. W. HONG and C. J. KIM, *Supercond. Sci. and Technol.* **9** (1996) 694.
21. R. MILTECH, M. MURAKAMI, A. PREISINGER and H. W. WEBER, *Physica C* **209** (1993) 415.
22. P. DIKO, M. AUSLOOS, R. CLOOTS, *ibid.* **235–240** (1994) 359.
23. "Melt Processed High-Temperature Superconductors," edited by M. Murakami (World Scientific, Singapore, 1992) p. 75.
24. P. DIKO, W. GAWALEK, T. HABISREUTHER, T. KLUPSCH and P. GORNET, *Phys. Rev. B* **52** (1995) 13658.
25. K. NO, D. YOON, W. S. SHIN, W. B. KIM and D. SHIM, *J. Mater. Sci.* **29** (1994) 2345.
26. C. J. KIM, K. B. KIM and G. W. HONG, *Physica C* **243** (1995) 366.
27. A. GOYAL, W. C. OLIVER, P. D. FUNKENBUSCH, D. M. KROEGER and S. J. BURNS, *ibid.* **183** (1991) 221.
28. P. DIKO, M. AUSLOOS and R. CLOOTS, *J. Mater. Res.* **11** (1995) 1179.
29. P. DIKO, W. GAWALEK, T. HABISREUTHER, T. KLUPSCH and P. GORNET, *Phys. Rev. B* **52** (1995) 13658.
30. M. CHOPRA, S. W. CHAN, R. L. MENG and C. W. CHU, *J. Mater. Res.* **11** (1996) 1616.
31. D. F. LEE, X. CHAUD and K. SALAMA, *Physica C* **181** (1991) 81.
32. N. OGAWA, I. HIRABAYASHI and S. TANAKA, *ibid.* **177** (1991) 101.
33. T. IZUMI, Y. NAKAMURA and Y. SHIOHARA, *J. Mater. Res.* **7** (1992) 1621.
34. E. SUDHAKAR REDDY and T. RAJASEKHARAN, *Supercond. Sci and Technol.* **11** (1998) 523.

Received 16 December 1997
and accepted 27 January 1999